

Electrochemical Performance of Graphene as Effected by Electrode Porosity and Graphene Functionalization

Christian Punckt,^a Michael A. Pope,^a Jun Liu,^b Yuehe Lin,^b Ilhan A. Aksay^{*a}

^a Department of Chemical and Biological Engineering, Princeton University, Princeton, NJ 08544, USA

^b Pacific Northwest National Laboratory, Richland, WA 99352, USA

phone: (609) 258-4393

*e-mail: iaksay@princeton.edu

Received: June 11, 2010

Accepted: July 13, 2010

Abstract

Graphene-based electrodes have recently gained popularity due to their superior electrochemical properties. However, the exact mechanisms of electrochemical activity are not yet understood. Here, we present data from NADH oxidation and ferri/ferrocyanide redox probe experiments to demonstrate that both (i) the porosity of the graphene electrodes, as effected by the packing morphology, and (ii) the functional group and the lattice defect concentration play a significant role on their electrochemical performance.

Keywords: Graphene, Sensors, Porosity, Functionalization, Catalysis

DOI: 10.1002/elan.201000367

1 Introduction

Carbon-based electrodes have been extensively studied because of their good electronic conductivity, chemical inertness, large potential window, and electrocatalytic activity for many important redox reactions [1]. For the preparation of such electrodes, usually an inert substrate, e.g., glassy carbon (GC), is coated with electrochemically active layers such as doped diamond [2–6], carbon nanotubes (CNTs) [7–9], graphene sheets (GSs) [10–16], and other micro- and nanoscale carbonaceous materials [1,17,18], often in combination with polymeric binders which improve sensor selectivity and prevent electrode fouling [19].

Despite the large number of studies that utilize the enhanced electrocatalytic activity of CNTs and GSs, the systematic analysis of the origin of the observed effects has just begun. In the majority of recent studies, results obtained with one type of carbon nanomaterial are not compared to more conventional materials such as carbon black (CB), although it has been shown that, for example for the oxidation of nicotinamid adenine dinucleotide (hydrogen) (NADH) and other biomolecules, CNTs do not exhibit a superior electrocatalytic effect compared to simple graphite powder [18].

Furthermore, Menshkykau and Compton in a theoretical work predicted that electrode packing morphology should also play a crucial role in the interpretation of cyclic voltammetry (CV) data [20]. From studies employing graphene for supercapacitor applications [21], it is known that such electrodes exhibit considerable porosity and have large specific surface areas which can strongly

affect the response of a sensor device. Consequently, we contend that the choice of carbon material and the coating method, such as capillary-force-induced (CFI) packing during evaporation of a graphene suspension or abrasive coating, should have a strong impact on the apparent electrochemical properties of the electrode due to resulting differences in electrode porosity.

In the following, we present a comparative study of the electrochemical properties of different types of GSs and CB which are coated onto glassy carbon substrates under CFI packing. We analyze the impact of both the chemical composition and the morphology of the electrode material on the electrochemical performance during the oxidation of NADH. For a better characterization of our electrodes, redox probe tests with ferro/ferri-cyanide are conducted. We focus on functionalized graphene sheets (FGSs) [22,23] as an active electrode material due to their unique chemical, thermal, electrical, and structural properties. Especially the ‘defectiveness’ of FGSs, i.e., the presence of functional groups and lattice defects (see Figure 1) [23–26], which differentiates them from pristine graphene, is expected to have important advantages for their use in electrochemical sensor devices.

Functional groups have been shown to be responsible for the electrochemical activity of carbonaceous nanomaterials by providing electrochemically active surface sites both on FGSs and CNTs, where redox reactions can be catalyzed [7,9,16,17] or enzymes can be attached for biosensor applications [12,19]. In the case of CNTs, it is commonly believed that only functional groups at the open ends of the tubes act as such active sites, similar to edge-plane pyrolytic graphite electrodes [27], and for gra-

phene-based electrodes, functional groups at the edges of the sheets can be expected to be of similar importance [10, 13, 14, 16]. Functionalized graphene, however, also exhibits a large density of defects within the carbon lattice (Figure 1) [25]. It has been shown that lattice defects significantly affect the electron transfer kinetics of CNTs [28–30] and graphite surfaces [31] although the defect density in these materials is low. Therefore, when comparing FGSs with other types of carbon materials, the increased density of lattice defects on FGSs is expected to play a significant role in their electrocatalytic properties. Furthermore, the fabrication of FGSs does not involve metal catalysts; and, thus artifacts caused by metal impurities (as observed in studies with CNTs [32–35]) can most likely be excluded.

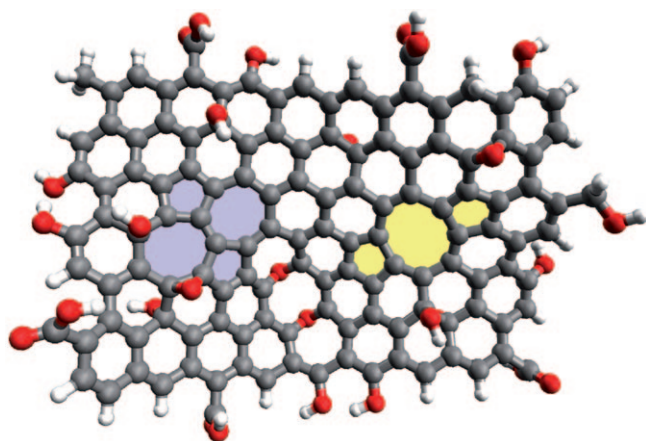


Fig. 1. Schematic of functional groups and lattice defects on FGSs showing epoxy and hydroxyl groups on both sides of the graphene plane, carboxyl and hydroxyl groups at the edges, a 5-8-5 defect (yellow), and a 5-7-7-5 (Stone–Wales) defect (blue). Carbon atoms are gray, oxygen atoms are red, and hydrogen atoms are white [25, 26].

Our results indicate that FGSs with carbon/oxygen ratio (C/O) ~ 15 show stronger electrocatalytic effects towards NADH oxidation compared to CNTs [9], chemically reduced graphite oxide (CRGO) [14], CB, and FGSs with much higher C/O (> 200) most likely due to a higher concentration of functional sites and/or lattice defects. We also show that electrode porosity needs to be taken into account as an important factor in comparing apparent electrocatalytic effects of porous electrode materials.

2 Experimental

As substrates for our electrode coatings, we employed GC electrodes with a diameter of 3 mm which were embedded in poly(chlorotrifluoroethylene) (PCTFE). Prior to either use in the experiment or subsequent coating with CB or FGSs, the GC electrodes were polished with a $0.05 \mu\text{m}$ gamma alumina particle suspension, washed in

de-ionized water, sonicated in ethanol, and dried under a stream of nitrogen. CB (Ketjenblack EC600) was used as purchased. The FGSs were produced as described elsewhere [23], typically with a C/O ratio of ~ 10 – 20 . To increase the C/O ratio further, FGS powder was heat treated at 1050°C in an atmosphere of 95% nitrogen and 5% hydrogen for 10 min., optionally followed by annealing at 1500°C in nitrogen for 2 min. We determined the C/O ratio of our coating materials by combustion-based chemical analysis (Atlantic Microlab Inc., GA). The C/O ratios for FGS, reduced (annealed) FGS, and CB were $14 \pm 5\%$, $\sim 350 \pm 25\%$ ($\sim 450 \pm 30\%$), and $\sim 220 \pm 20\%$, respectively. To distinguish the composition of the FGSs, we designate them as FGS_x , where x denotes the C/O ratio. CB and FGSs were suspended either in ethanol or in ammoniated deionized (DI) water (pH 11) at a concentration of typically 0.1 mg/mL and tip-sonicated for 30 min. in order to obtain a stable suspension.

The GC electrodes were coated by evaporating $\sim 50 \mu\text{L}$ of suspension on the electrode surface and drying in a nitrogen atmosphere over night. FGS suspensions in ammoniated DI water were applied by repeatedly coating the electrode with about $5 \mu\text{L}$ of suspension. Each layer was allowed to dry before the next application. This procedure ensured that only the GC and not the PCTFE was wetted by the suspension. The resulting surface coatings were adherent to the surface of the GC electrode and could not be rinsed off under a stream of water.

The porosity and surface area of the films deposited from ethanol- and water-based suspensions were analyzed by measuring mass accumulation/reduction isotherms of benzene on graphene coatings, as a function of partial pressure of benzene in the gas phase [36–38] measured by a quartz crystal microbalance (QCM) technique [39, 40]. The electrode coating procedure described above was applied to gold coated QCMs which were placed in a homemade gas flow cell. Dry nitrogen was bubbled through benzene and the saturated vapor was mixed with a stream of pure nitrogen. The partial pressure of benzene was varied by changing the relative flow rates entering a mixing chamber from where the vapor was sent to the QCM cell. The concentration of benzene in the gas stream was monitored by Fourier transform infrared (FTIR) spectroscopy. The partial pressure was determined by taking the ratio of the absorbance at 3050 cm^{-1} for the gas mixture to the absorbance of saturated benzene vapor measured before and after recording each isotherm.

Electrochemical experiments were conducted in 5 mL of 50 mM phosphate buffer saline (PBS) at pH 7.4 using a computer-controlled digital potentiostat (VSP, Bio-Logic USA, Inc.). A platinum wire served as counter electrode and all potentials were measured versus a Ag/AgCl reference electrode. Before each experiment, the electrolyte was purged with nitrogen for 15 min. During the experiments, the nitrogen line was pulled out of the electrolyte to avoid convection but remained inside the electrochemical cell to provide an inert gas atmosphere.

3 Results and Discussion

In Figure 2, we show the CV data obtained with four different types of electrodes. As expected, the modification of the GC electrode with various carbons caused the NADH oxidation peak to shift towards smaller potentials compared to the bare GC surface. The peak shifts observed with FGS₃₅₀ and CB are approximately the same (~250 mV) and smaller than the peak shift observed with FGS₁₅ (>300 mV). Therefore, the FGS₁₅-modified electrode possesses the largest electrocatalytic activity towards NADH oxidation. A likely explanation for this is the larger density of lattice defects and functional groups such as carboxyl, epoxy, and hydroxyl groups of FGS₁₅ compared to FGS₃₅₀ and CB. Presently, it is not clear whether the functional sites or the lattice defects play a more prominent role on the electrochemical activity because the C/O ratio is only a global measure of the graphene structure, and the reduction and annealing of FGSs both reduce the density of functional groups and decrease the number of lattice defects (annealing) [25,41]. To understand the role of specific functional groups and lattice defects, characterization techniques such as Raman spectroscopy are needed for more in-depth studies.

Furthermore, the main goal of this manuscript is to show that the porosity of the electrodes and the resultant tortuosity can have a profound effect on the electrochemical response of graphene electrodes as well. Below, we provide experimental support for the concepts pointed out in the literature [42,43] and more recently studied theoretically by Menshykau and Compton [20], that differences in packing morphology of the electrodes have a significant impact on electrode performance. An indication for the existence of such differences in the data shown in Figure 2 is, for example, the observation of varying capacitive background currents. The effect of different transport rates as effected by the tortuosity of the carbon powder compacts must be taken into account before a firm conclusion about their electrocatalytic properties can be made.

3.1 Electrode Porosity Factor

In order to characterize our electrode coatings in more detail, we performed CV experiments with the ferri/ferrocyanide couple employing various electrode coatings and determined the forward oxidation peak height I_{\max} and the peak-to-peak separation E_{pp} (see Figure 3). For a fast electrochemical reaction on a planar electrode in stagnant electrolyte, I_{\max} is proportional to the square root of the applied scan rate, ν since the reaction is controlled by diffusive transport of the involved educts and products [44]. In Figure 4a, we compare I_{\max} as a function of ν for two FGS₁₅-modified electrodes and a plain GC electrode. While the peak height shows the expected behavior for the plain GC electrode and the coating based on ammoniated DI water suspension, I_{\max} increases more strongly with increasing scan rate when the ethanol-based coating

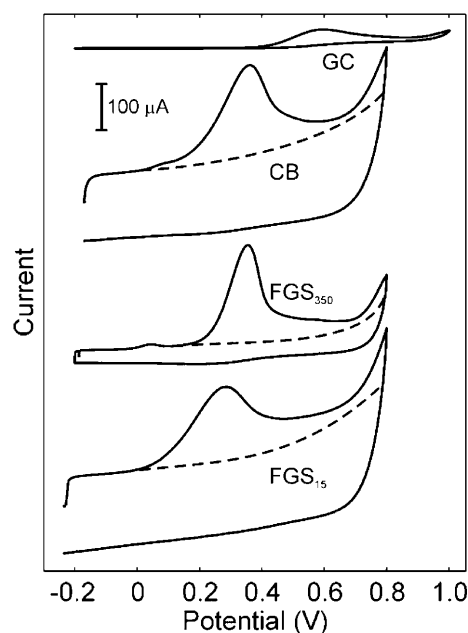


Fig. 2. Comparison of CVs of FGS-modified, CB-modified, and plain GC electrodes in a 50 mM PBS containing 5 mM NADH (dashed lines schematically indicate the shape of CVs in the absence of NADH). Electrode coatings were prepared from ethanol suspensions. Scan rate: $\nu = 100$ mV/s, potential measured vs. Ag/AgCl.

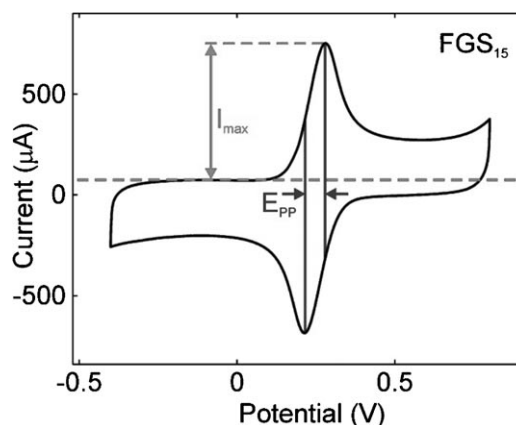


Fig. 3. Cyclic voltammogram obtained with 5 mM ferrocyanide in PBS at a scan rate of 100 mV/s using a GC electrode coated with FGSs from an ethanol suspension. Indicated are the forward oxidation peak height I_{\max} and the peak-to-peak separation E_{pp} . Note that the value of I_{\max} is measured with respect to the capacitive background current.

is employed. Menshykau and Compton predicted that the over-proportional increase of the oxidation current can be explained by electrode porosity [20]. While at large scan rates, the diffusion layer thickness does not exceed the average pore radius and the full surface area of the porous electrode is involved in the electrochemical reaction, at low scan rates the diffusion layer thickness increases to such an extent that the pores are depleted of

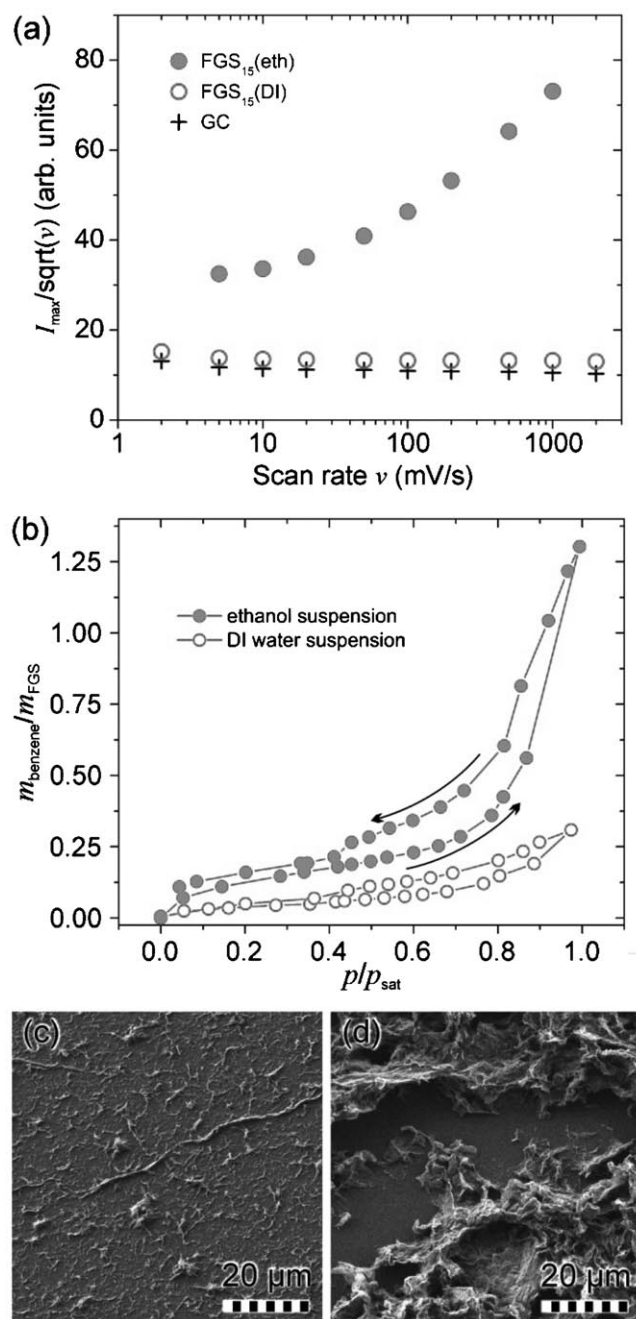


Fig. 4. a) Peak current I_{\max} as function of scan rate v for a plain GC electrode and electrodes coated with FGS₁₅ using a DI-water-based (DI) and an ethanol-based (eth) suspension. b) Benzene mass accumulation/reduction isotherms on FGS₁₅ films prepared from DI-water-based and ethanol-based suspensions. Black arrows indicate the direction of the measurement. SEM images below show coated electrode surfaces using c) ammoniated DI water and d) ethanol.

the reactant and only the topmost regions of the electrode which are in close vicinity to the bulk electrolyte are involved in the reaction.

We characterized the morphology of dried FGS films corresponding to the different electrode types shown in Figure 4a by measuring mass accumulation/reduction iso-

therms of benzene. For determining the surface area and pore size distribution of porous carbonaceous materials, this method has been intensively studied and widely used [36,38,45–48]. In Figure 4b, we show the adsorbed mass of benzene per mass of FGSs (both measured using the QCM) as a function of the benzene partial pressure, p to which the FGS film was exposed measured as the fraction of the saturation pressure p_{sat} . The curves show a typical shape (type IV) [38,49] that is commonly observed in the literature [36,48]. At low benzene partial pressures ($p/p_{\text{sat}} < \sim 0.35$), the mass accumulation (with increasing p) and reduction (with decreasing p) isotherms are due to gas adsorption and desorption and can be analyzed by the Brunauer-Emmett-Teller (BET) equation [39,50]. The specific BET surface areas of the films dried from ethanol and DI-water suspensions are about 350 and 150 m²/g, respectively. At larger partial pressures, the mass accumulation increases strongly, and upon subsequent reduction of p a hysteresis is observed during mass reduction. Both observations are typical for condensation and evaporation inside a porous network [38,39]. The hysteresis associated with mass accumulation and reduction is more pronounced for the FGS film made by the evaporation of ethanol suspension, indicating a larger fraction of mesopores [38,39,51] in this material as compared to the DI-water-based film.

Figures 4c,d show scanning electron microscopy (SEM) images of the two corresponding FGS electrode coatings fabricated by CFI packing of FGS₁₅ in ammoniated DI water (Figure 4c) and in ethanol (Figure 4d), respectively. The information we obtain from imaging is rather qualitative; however, the images suggest that the layer generated from ethanol suspension exhibits a larger amount of macropores as compared to the DI-water-based electrode film.

We have thus correlated the appearance of the over-proportional increase of I_{\max} shown in Figure 4a for the ethanol suspension-based electrode coating with the occurrence of increased specific surface area and porosity as determined by benzene accumulation isotherms (Figure 4b) and with apparent morphological differences in electron microscopy images (Figures 4c,d). This indicates that our electrochemical results are indeed influenced by the porosity effects predicted by Menshkykau and Compton [20].

We suggest that the differences in film morphology are due to the different drying behavior of ethanol and DI water suspensions as effected by the differences in the interfacial energies of the liquids: During the evaporation of a droplet of ethanol suspension both on the GC electrode and on the QCMs employed for mass accumulation measurements, we observe a partial aggregation of FGS inside the droplet and the formation of a rather thick layer of FGS. On the other hand, the evaporation of DI water suspension on either substrate results in the formation of a surface layer of FGS already on the suspension droplet. Eventually, this layer is deposited as a dense film on the electrode surface (see Figures 4c,d).

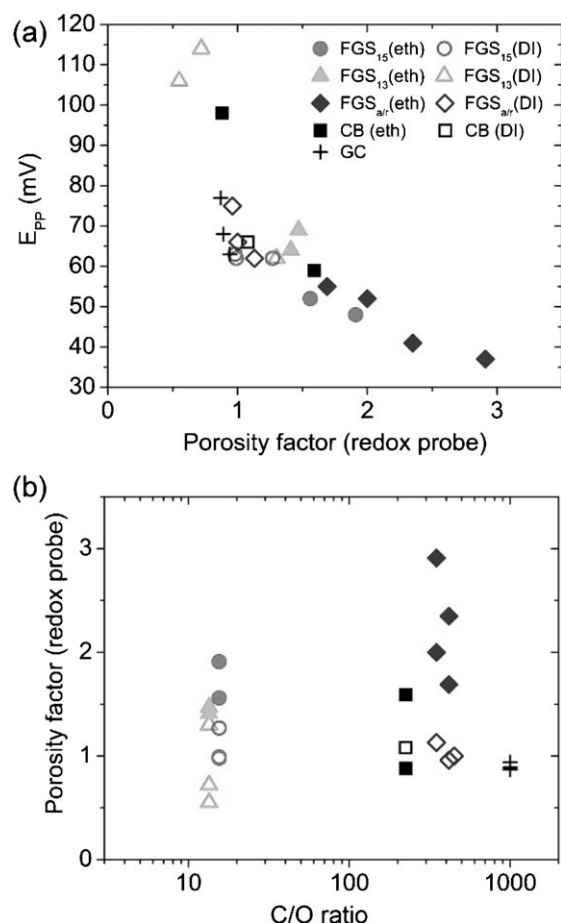


Fig. 5. a) E_{pp} as a function of the porosity factor (see text). b) Porosity factor as a function of the C/O ratio of the electrode material. We assigned the arbitrary value of 1000 to the C/O ratio of plain GC. The legend in (a) refers to both panels (a) and (b). Closed (open) symbols refer to electrode coatings based on ethanol (ammoniated DI water). FGS_{air} refers to the different batches of thermally annealed and reduced FGSs with C/O ratios between 350 and 450.

For our electrochemical measurements, we define an ‘electrochemical’ measure for the porosity of our electrodes in the following way: From a series of CV data with varying scan rate ν , we obtain the value of I_{max} at $\nu = 10$ mV/s and $\nu = 500$ mV/s and calculate a porosity factor P according to the equation

$$P = k \cdot \frac{I_{max}(\nu = 500 \text{ mV/s})}{I_{max}(\nu = 10 \text{ mV/s})} \quad \text{with} \quad k = \frac{\sqrt{10}}{\sqrt{500}}$$

For an ideal planar electrode, $P=1$ since then $I_{max} \sim (\nu)^{1/2}$. Measurements with electrodes exhibiting a stronger increase of the peak current due to porosity effects should result in a CV data series with $P > 1$. While this is a rather primitive measure of electrode morphology, we can show that it is still indicative of the electrochemical performance of the electrode film.

In Figure 5a, we plot E_{pp} as a function of P for various electrode coatings and plain GC. A negative correlation of E_{pp} and P is observed: The smallest peak-to-peak separation is found for electrodes with the largest porosity factor. The same behavior has also been pointed out in Menshukau and Compton’s theoretical study [20]: In porous electrode structures, the transport of reaction educts can be facilitated to such an extent that even for infinitely fast electron kinetics a decrease of the separation between oxidation and reduction peak is observed indicating ‘electrocatalytic’ activity of the electrode. The similarity of our experimental results and the theoretical prediction further supports our approach to employ P as a measure of electrode porosity. Interestingly, there is a strong dependence of E_{pp} and P on the dispersion medium. The largest porosity factors and the smallest peak-to-peak separations are observed with electrode coatings made from an ethanol suspension. On the other hand, electrode coatings fabricated from DI water suspensions do not exceed the performance of the plain GC electrodes significantly. This observation corresponds to the differences in film porosity as measured by benzene mass accumulation (Figure 4b) and indicated by SEM imaging (Figures 4c,d).

3.2 The Effect of Graphene Composition as Measured by the C/O Ratio

The porosity factor depends only weakly on the C/O ratio of the coating material (Figure 5b). For most materials tested, an ethanol suspension of the individual material resulted in substantially larger values of P than the corresponding DI water suspension. However, for the ethanol-based FGS suspensions, we observe that higher C/O ratio results in slightly increased P . This might be due to the increased hydrophobicity of FGSs with high C/O ratio and resulting differences in dispersion stability during drying. Since the drying process on the electrodes is not well controlled, the scatter in the data is large, and a more systematic study of these effects, employing FGS monolayers will be the subject of future work.

We measured the NADH oxidation potential E_{NADH} as a function of P (Figures 6a,b) and did not observe an obvious trend as has been seen for E_{pp} of the redox probe experiments (Figure 5a). In Figure 6a, we show E_{NADH} as a function of the porosity factor which has been obtained during a redox probe experiment immediately preceding the NADH measurement. Electrode porosity had no obvious impact on E_{NADH} . A plain GC electrode resulted in the largest E_{NADH} while electrodes coated with different suspensions of low C/O ratio FGS resulted in a strongly reduced overpotential. For each individual type of coating, however, the effects of dispersion medium and (correlated with that) electrode porosity are still present: For example, the three data points corresponding to a DI water suspension of reduced and annealed FGS (open diamonds in Figure 6a) are located at a larger overpotential

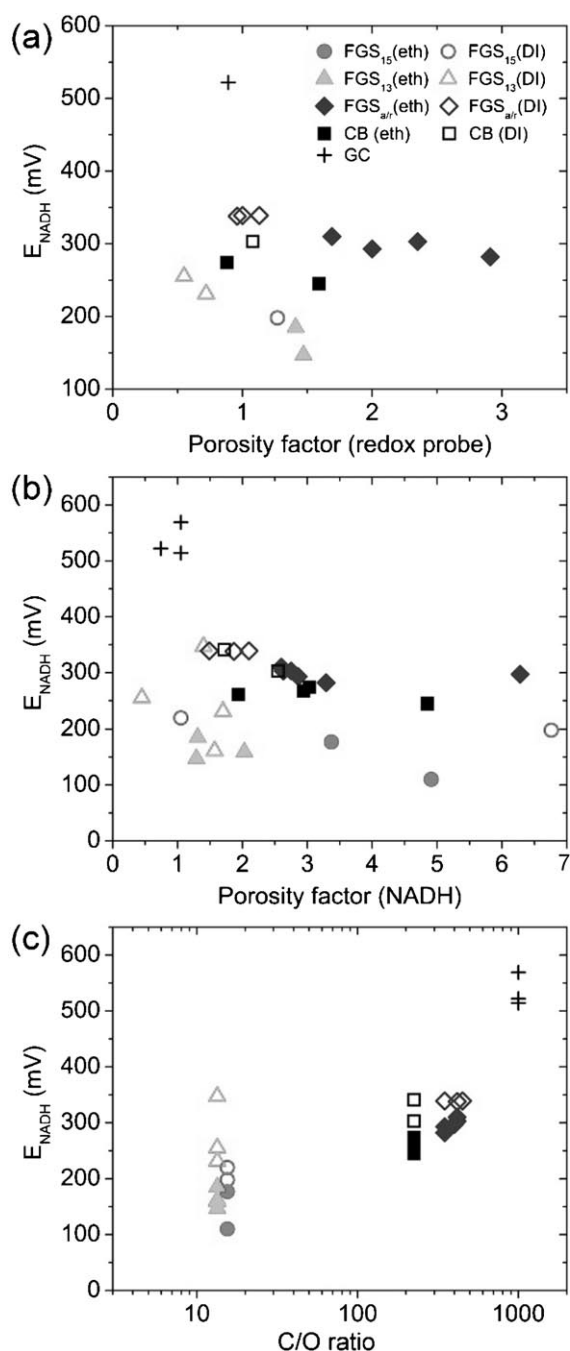


Fig. 6. NADH oxidation overpotential E_{NADH} plotted as a function of P , P_{NADH} (see text) and C/O ratio. The legend in (a) refers to panels (a–c) and corresponds to the legend used in Figure 5a.

than the data points corresponding to the ethanol suspension of the same material (filled diamonds).

To increase the amount of data points in our analysis, we also took measurements into consideration which had been performed with electrodes that were not tested with the ferri/ferrocyanide couple prior to the NADH experiment. For these measurements, we calculated a porosity factor P_{NADH} based on I_{max} obtained from the NADH measurement itself. In Figure 6b, we show these data

points together with the data presented in Figure 6a (for which we also calculated P_{NADH} from the NADH response). Again, no correlation between E_{NADH} and the electrode porosity can be seen, and electrode coatings with low C/O ratio result in reduced overpotential. The overall behavior is thus similar as for the data shown in Figure 6a. However, NADH can certainly not be expected to behave like an ideal redox probe since its oxidation involves complicated charge transfer processes [52,53], and porosity estimates based on the change of the NADH oxidation peak currents with scan rate are probably affected by effects other than only the electrode morphology.

The dependence of the results on the C/O ratio of the electrode coating is more clearly shown in Figure 6c. Overpotentials as low as 100 mV vs. Ag/AgCl were measured with electrode coatings of FGS₁₅. All electrode materials with larger C/O ratio showed substantially smaller potential shifts compared to the plain GC electrode. It should be noted that employing FGSs with C/O ratios approaching a value of 2 is expected to result in strongly decreased, if any, electrode performance due to transition from an electrically conducting to an insulating state [54]. In this case, the large density of functional groups and defects cause a decrease in the conductivity of the FGSs such that significant ohmic losses will occur within the FGS network during electrode operation. The dispersion medium used during the electrode coating process – and related to that the electrode porosity – has an additional impact on the results shown in Figure 6c as can be seen from the fact that all open symbols (corresponding to DI water suspensions) are located at higher overpotentials than the corresponding filled symbols (corresponding to ethanol suspensions).

4 Conclusions

We have demonstrated that using low C/O ratio, electrically conducting FGSs as sensor electrode causes a decrease of the overpotential for the electrochemical oxidation of NADH which is larger than that observed for all other tested materials. Due to our detailed comparison and systematic study of the impact of electrode morphology, we conclude that the increased electrocatalytic activity of FGSs is likely due to their large density of both functional groups and lattice defects compared to other types of carbon-based nanomaterials. The presence of a correlation between the electrode porosity factor P , the surface morphology as characterized by benzene adsorption, and the peak-to-peak separation E_{pp} in the redox probe data supports the idea that electrode morphology and, more specifically, electrode porosity has a significant impact on the result of an electrochemical experiment. Electrode porosity, as defined by the porosity factor P , has an ‘amplifying’ effect on the apparent electrocatalytic behavior of porous graphene- and carbon black-coated electrodes.

Our results suggest that porosity-related effects play an important role in the interpretation of electrocatalytic behavior observed at porous electrodes in general. Since such behavior can at least in part be caused by morphology effects rather than by 'true' electrocatalysis, a comparison of different materials without a simultaneous analysis of the electrode morphology effects may lead to misleading results.

Acknowledgements

This work was supported by an Army Research Office (ARO)/Multidisciplinary Research Initiative (MURI) under Grant Number W911NF-09-1-0476 and the Directed Technologies, Inc. The research at the Pacific Northwest National Laboratory (PNNL) was supported by a PNNL Laboratory Directed Research and Development project. PNNL is operated for the U.S. Department of Energy (DOE) by Battelle under Contract DE-AC05-76RL01830. CP acknowledges support from the Alexander von Humboldt Foundation.

References

- [1] R. L. McCreery, *Chem. Rev.* **2008**, *108*, 2646.
- [2] Y. L. Zhou, J. F. Zhi, *Talanta* **2009**, *79*, 1189.
- [3] T. L. Lasseter, B. H. Clare, N. L. Abbott, R. J. Hamers, *J. Am. Chem. Soc.* **2004**, *126*, 10220.
- [4] A. Hartl, E. Schmich, J. A. Garrido, J. Hernando, S. C. R. Catharino, S. Walter, P. Feulner, A. Kromka, D. Steinmüller, M. Stutzmann, *Nat. Mater.* **2004**, *3*, 736.
- [5] A. Fujishima, T. N. Rao, E. Popa, B. V. Sarada, I. Yagi, D. A. Tryk, *J. Electroanal. Chem.* **1999**, *473*, 179.
- [6] T. N. Rao, I. Yagi, T. Miwa, D. A. Tryk, A. Fujishima, *Anal. Chem.* **1999**, *71*, 2506.
- [7] G. G. Wildgoose, C. E. Banks, H. C. Leventis, R. G. Compton, *Microchim. Acta* **2006**, *152*, 187.
- [8] J. Wang, M. Musameh, Y. H. Lin, *J. Am. Chem. Soc.* **2003**, *125*, 2408.
- [9] M. Musameh, J. Wang, A. Merkoci, Y. H. Lin, *Electrochem. Commun.* **2002**, *4*, 743.
- [10] Y. Shao, J. Wang, H. Wu, J. Liu, I. A. Aksay, Y. Lin, *Electroanalysis* **2010**, *22*, 1027.
- [11] Y. Wang, Y. M. Li, L. H. Tang, J. Lu, J. H. Li, *Electrochem. Commun.* **2009**, *11*, 889.
- [12] X. H. Kang, J. Wang, H. Wu, I. A. Aksay, J. Liu, Y. H. Lin, *Biosens. Bioelectron.* **2009**, *25*, 901.
- [13] J. F. Wang, S. L. Yang, D. Y. Guo, P. Yu, D. Li, J. S. Ye, L. Q. Mao, *Electrochem. Commun.* **2009**, *11*, 1892.
- [14] M. Zhou, Y. M. Zhai, S. J. Dong, *Anal. Chem.* **2009**, *81*, 5603.
- [15] S. Alwarappan, A. Erdem, C. Liu, C. Z. Li, *J. Phys. Chem. C* **2009**, *113*, 8853.
- [16] W. J. Lin, C. S. Liao, J. H. Jhang, Y. C. Tsai, *Electrochem. Commun.* **2009**, *11*, 2153.
- [17] C. E. Banks, T. J. Davies, G. G. Wildgoose, R. G. Compton, *Chem. Commun.* **2005**, 829.
- [18] R. R. Moore, C. E. Banks, R. G. Compton, *Anal. Chem.* **2004**, *76*, 2677.
- [19] J. Wang, *Electroanalysis* **2005**, *17*, 7.
- [20] D. Menshkyau, R. G. Compton, *Electroanalysis* **2008**, *20*, 2387.
- [21] M. D. Stoller, S. J. Park, Y. W. Zhu, J. H. An, R. S. Ruoff, *Nano Lett.* **2008**, *8*, 3498.
- [22] M. J. McAllister, J. L. Li, D. H. Adamson, H. C. Schniepp, A. A. Abdala, J. Liu, M. Herrera-Alonso, D. L. Milius, R. Car, R. K. Prud'homme, I. A. Aksay, *Chem. Mater.* **2007**, *19*, 4396.
- [23] H. C. Schniepp, J. L. Li, M. J. McAllister, H. Sai, M. Herrera-Alonso, D. H. Adamson, R. K. Prud'homme, R. Car, D. A. Saville, I. A. Aksay, *J. Phys. Chem. B* **2006**, *110*, 8535.
- [24] W. Gao, L. B. Alemany, L. J. Ci, P. M. Ajayan, *Nat. Chem.* **2009**, *1*, 403.
- [25] K. N. Kudin, B. Ozbas, H. C. Schniepp, R. K. Prud'homme, I. A. Aksay, R. Car, *Nano Lett.* **2008**, *8*, 36.
- [26] H. C. Schniepp, K. N. Kudin, J. L. Li, R. K. Prud'homme, R. Car, D. A. Saville, I. A. Aksay, *ACS Nano* **2008**, *2*, 2577.
- [27] C. E. Banks, R. R. Moore, T. J. Davies, R. G. Compton, *Chem. Commun.* **2004**, 1804.
- [28] I. Dumitrescu, P. V. Dudin, J. P. Edgeworth, J. V. Macpherson, P. R. Unwin, *J. Phys. Chem. C* **2010**, *114*, 2633.
- [29] A. F. Holloway, G. G. Wildgoose, R. G. Compton, L. D. Shao, M. L. H. Green, *J. Solid State Electrochem.* **2008**, *12*, 1337.
- [30] Y. W. Fan, B. R. Goldsmith, P. G. Collins, *Nat. Mater.* **2005**, *4*, 906.
- [31] J. K. Kariuki, M. T. McDermott, *Langmuir* **1999**, *15*, 6534.
- [32] M. Pumera, H. Iwai, Y. Miyahara, *ChemPhysChem* **2009**, *10*, 1770.
- [33] L. Siegert, D. K. Kampouris, J. Kruusma, V. Sammelselg, C. E. Banks, *Electroanalysis* **2009**, *21*, 48.
- [34] C. Batchelor-McAuley, G. G. Wildgoose, R. G. Compton, L. D. Shao, M. L. H. Green, *Sens. Actuators B, Chem.* **2008**, *132*, 356.
- [35] B. Sljucic, C. E. Banks, R. G. Compton, *Nano Lett.* **2006**, *6*, 1556.
- [36] P. A. Gauden, A. P. Terzyk, G. Rychlicki, P. Kowalczyk, K. Lota, E. Raymundo-Pinero, E. Frackowiak, F. Beguin, *Chem. Phys. Lett.* **2006**, *421*, 409.
- [37] M. M. Dubinin, H. F. Stoeckli, *J. Colloid Interf. Sci.* **1980**, *75*, 34.
- [38] S. J. Gregg, K. S. W. Sing, *Adsorption, Surface Area and Porosity*, Academic Press, London **1982**.
- [39] S. H. Bhansali, J. M. Jarvis, I. A. Aksay, J. D. Carbeck, *Langmuir* **2006**, *22*, 6676.
- [40] V. Tsionsky, E. Gileadi, *Langmuir* **1994**, *10*, 2830.
- [41] K. Sato, R. Saito, Y. Oyama, J. Jiang, L. G. Cancado, M. A. Pimenta, A. Jorio, G. G. Samsonidze, G. Dresselhaus, M. S. Dresselhaus, *Chem. Phys. Lett.* **2006**, *427*, 117.
- [42] L. G. Austin, *Trans. Faraday Soc.* **1964**, *60*, 1319.
- [43] Y. A. Chizmadzhev, Y. G. Chirkov, in *Comprehensive Treatise of Electrochemistry* (Eds: E. Yeager, J. O. M. Bockris, B. E. Conway, S. Sarangapani), Plenum Press, New York **1983**.
- [44] R. G. Compton, *Understanding Voltammetry*, World Scientific, London **2007**.
- [45] G. Gryglewicz, J. Machnikowski, E. Lorenc-Grabowska, G. Lota, E. Frackowiak, *Electrochim. Acta* **2005**, *50*, 1197.
- [46] D. D. Do, C. Nguyen, H. D. Do, *Colloids Surf. A* **2001**, *187*, 51.
- [47] M. Eswaramoorthy, R. Sen, C. N. R. Rao, *Chem. Phys. Lett.* **1999**, *304*, 207.
- [48] C. Moreno-Castilla, J. Rivera-Utrilla, F. Carrasco-Marin, M. V. Lopez-Ramon, *Langmuir* **1997**, *13*, 5208.
- [49] S. Brunauer, L. S. Deming, W. E. Deming, E. Teller, *J. Am. Chem. Soc.* **1940**, *62*, 1723.

- [50] S. Brunauer, P. H. Emmett, E. Teller, *J. Am. Chem. Soc.* **1938**, *60*, 309.
- [51] E. P. Barrett, L. G. Joyner, P. P. Halenda, *J. Am. Chem. Soc.* **1951**, *73*, 373.
- [52] L. Gorton, *J. Chem. Soc. Faraday Trans. 1* **1986**, *82*, 1245.
- [53] J. Moiroux, P. J. Elving, *J. Am. Chem. Soc.* **1980**, *102*, 6533.
- [54] C. Mattevi, G. Eda, S. Agnoli, S. Miller, K. A. Mkhoyan, O. Celik, D. Mostrogiovanni, G. Granozzi, E. Garfunkel, M. Chhowalla, *Adv. Funct. Mater.* **2009**, *19*, 2577.

Life's Simple Pleasures!



No need to waste precious time looking for the right information – Register now for the free **Wiley-VCH Alerting Service**.

It's simple – and it's fast.

To receive regular news per e-mail tailored precisely to your needs and interests, just fill in the registration form at www.wiley-vch.de/home/pas/

 **WILEY-VCH**